Effect of ion implantation on stripe- and bubble-domain coercivity

M. Pardavi-Horváth
Central Research Institute of Physics, H-1525 Budapest 114, P.O.B.49, Hungary

G. Vértesy
Hungarian Optical Works, H-1525 Budapest, P.O.B.52, Hungary

(Received 7 May 1985; accepted for publication 12 November 1985)

The static coercivity of stripe and bubble domains in 5-μm $(YSmCa)_3(FeGe)_5O_{12}$ epitaxial garnet films was measured by the oscillating-wall method. The dependence of coercivity on Ne^+ implantation energy and dosage was investigated. In a wide range of energy and dosage, implantation was found to eliminate hard bubbles and decrease bubble coercivity by 25%; the decrease is a measure of the contribution of Bloch lines to coercivity. The average number of Bloch lines n in bubble walls was determined from static coercivity as $37 \leqslant n \leqslant 62$, n increasing with quality factor Q. Bubble coercivity was always found to be higher than stripe coercivity measured by the same method. Implantation has no measurable effect on apparent stripe coercivity which may be a consequence of the lower Bloch line density of stripes relative to bubbles.

I. INTRODUCTION

A new type of cylindrical magnetic domain, the "hard bubble," was reported by Tabor *et al.* in 1972.[1] The collapse field of such anomalous bubbles is higher than that of normal bubbles, and they propagate at an angle to the applied gradient field. It was shown that these peculiarities are connected with the structure of the domain walls which are not simple, divergence-free 180° Bloch walls, but contain alternating Bloch- and Néel-type segments. Néel segments behave like a wall between the Bloch segments, and are known as Bloch lines. The presence of Bloch lines distinguishes a hard wall from a normal one, and there is an increase of the domain-wall energy in hard walls due mainly to the exchange energy of the Bloch lines—as was shown by Rosencwaig, Tabor, and Nelson[2] and Thiele.[3]

Hard bubbles are detrimental to bubble memory devices, and the routine technology for their suppression is ion implantation.[4] A dosage of 10^{14} Ne^+ ions/cm^2 at 80–100 keV energy completely eliminates hard bubbles in epitaxial garnet films with bubbles in the 1–5-μm range.[5] However, Bloch lines are also present in the hard-stripe walls, and the possible use of Bloch lines for information storage has revived the interest in stripe domains.[6] The dynamic behavior of stripe walls containing Bloch lines was shown to be similar to that of hard bubbles,[7] and it was proposed[8] that the contribution of Bloch lines to the stripe-wall energy has the form of an additive factor proportional to the density of Bloch lines, i.e., to the (revolution number)/(wall length) ratio.

The number of Bloch lines in as-grown, common bubble memory materials can vary in very wide limits. Jindal and Castro[9] found that $(YSmLuCa)_3(FeGe)_5O_{12}$ garnets always have multiple bubble states. This observation is in contrast to that of Tumelty, Singh, and Gilleo[10] who found bubbles predominantly with one pair of Bloch lines in as-grown, high-mobility $(YSmCa)_3(FeGe)_5O_{12}$ films. It is known that the tendency for the presence of hard bubbles decreases with decreasing quality factor Q ($= K/2\pi M_s^2$, where K is the uniaxial anisotropy energy density and M_s is the spontaneous magnetization of the film). Patterson[11] investigated hard-bubble coercivity for 5–7-μm bubbles in $(YEu)_3(FeGa)_5O_{12}$ epitaxial garnet films with 30–100 Bloch lines and established that the coercivity increased with increasing Bloch line density due to increased wall energy.

The increased energy of hard walls gives rise to increased coercivities H_c because coercivity results from local changes of the wall energy σ; i.e., $H_c \sim d\sigma/dx$. The need to modify existing theories of domain-wall dynamics to include coercivity is implicit in making possible any comparison of theoretical results with experiments. Nevertheless, coercivity is often ignored in various model calculations. Moreover, in the literature one can find various definitions and methods of measurement of coercivity. The confusion about H_c becomes pronounced in bubble dynamics, as there is a need to measure coercivity on moving bubbles to simulate the operation of bubble devices. However, it is not clear that stripe and bubble coercivities are equal, taking into account, for example, simple geometrical arguments contrasting the wall areas and the curvature ratios of stripes and bubbles. In addition, there seem to be no data on the relationship between coercivities for the same geometry of domain walls with and without Bloch lines. These circumstances led us to investigate the coercivity of stripes and bubbles by the same quasistatic method of wall oscillation in samples with and without Bloch lines, i.e., before and after ion implantation.

II. EXPERIMENTS

For the investigations, epitaxial garnet films of the well-known common bubble material $(YSmCa)_3(FeGe)_5O_{12}$ were chosen. Films were grown by liquid-phase epitaxy (LPE) on [111]-oriented 5-cm-diam GGG substrates. The parameters of the films were measured by standard methods for bubble film characterization.[12]

The epitaxial garnet film on the back of each substrate was removed prior to the measurements, and the wafers were cut into 7–16 samples. Different samples from the same film were implanted under different conditions. Five series of experiments were carried out on samples from five different films. Samples of four films (nos. 1–4 in Table I) were implanted with 80-keV Ne^+ ions with dosage ranging from 6×10^{12} to 6×10^{16} ions/cm^2. Samples of film no. 5 were implanted with the same 6×10^{14} ions/cm^2 dose but at different energies of Ne ions from 20 to 120 keV.

 0021-8979/86/062119-06$02.40

TABLE I. Properties of the measured SmCaGeYIG epitaxial garnet films (h,film thickness; p_0, zero-field stripe period; d, bubble diameter in H_c^b measurements; H_0, bubble collapse field, $4\pi M_s$, saturation magnetization; K_u, uniaxial anisotropy constant; Q, quality factor).

Film no.	h (μm)	p_0 (μm)	d (μm)	H_0 (Oe)	$4\pi M_s$ (G)	K_u 10^3erg/cm^3	Q
1	5.3	9.2	4.3	118	200	7	4.4
2	4.6	12.2	5.6	77	181	12	9.3
3	5.4	10.7	5.2	101	198	10	6.7
4	4.2	9.5	4.8	100	213	13	7.0
5	5.1	10.9	5.8	94	196	12	7.6

The static coercivity H_c^{ij} (where $i = s,b$ and $j = 0,i$ in the upper indices denote coercivity measured on stripes or bubbles and on nonimplanted or implanted samples, respectively) was measured by the low-frequency wall-oscillation method (in zero external bias field[13]) and on bubble domains by the same method in the presence of a static bias field H_b ($H_{\text{stripe out}} < H_b < H_0$). Bubbles were generated by field pulses which cut stripes. Measurements were performed at room temperature. The coercivities of each sample were measured before and after implantation.

The collapse-field range ΔH_0, i.e., the difference in bias fields at which the first and the last bubbles collapse in a given sample, was visually measured.

III. RESULTS

Film properties were typical of 5-μm bubble materials, except for the coercivity, which varied among the measured films from 0.3 to 3 Oe, and for Q, which varied between 4 and 9; this latter feature enabled us to use high-Q approximations. The properties of the measured garnet films are given in Table I.

The measured values of stripe and bubble coercivities (H_c^s,H_c^b) averaged over 7–16 samples from every film and the effect of ion implantation on the coercivity are summarized in Table II. The scatter of the data is about 5%, which is within the error limits of the measurements on unimplanted stripes and bubbles, and it reaches 10% in some cases for implanted bubble coercivities H_c^{bi}. The value of H_c^b decreases as a consequence of implantation, whereas the stripe coercivity H_c^s is seemingly not influenced by implantation. The coercivity measured on stripes is always smaller than the coercivity measured on bubbles.

The average ratio of bubble-domain coercivities for unimplanted and implanted samples is similar for every film; its average value is $H_c^{bi}/H_c^{b0} = 0.76 \pm 0.02$ for 53 samples in spite of the fact that the measured films have significantly different coercivities.

The effect of an implanted dose on H_c^b is illustrated for two films (nos. 1 and 3 of Table I), one with low H_c and one with high H_c (Fig. 1). It is seen that H_c^{bi}—the bubble coercivity of implanted samples—does not depend on the implanted dose in a very wide range from 6×10^{12} to 6×10^{16} Ne^+ ions/cm^2. Data points for unimplanted samples plotted versus dosage mean that measurements were made on the same samples before implantation. Figure 2 shows the implantation energy dependence of H_c^b; crosses denote unimplanted samples, as above. The decrease of the coercivity does not depend on the energy of Ne ions between 40 and 120 keV.

The effectiveness of ion implantation is usually measured by the disappearance of hard bubbles appearing in the change of the collapse field distribution range; when $\Delta H_0 < 2$ Oe, the implantation is regarded as adequate. The distribution range of the collapse field ΔH_0 for film no. 1 can be seen as a function of the dose of the implantation at 80 keV energy of Ne^+ ions in Fig. 3. It is noticeable that the window for the disappearance of hard bubbles is narrower than the range of the decrease of the coercivity, as it is evident from the comparison of Figs. 1 and 3. The coercivity H_c^{bi} does not change up to the highest dose of 6×10^{16} Ne^+ ions/cm^2, whereas ΔH_0 starts to increase at a dose which is lower by 2 orders of magnitude.

IV. DISCUSSION

Conditions for hard-bubble suppression by ion implantation are well known although our present understanding of the mechanism is not complete. Implantation creates an approximately 0.1-μm-thick surface layer with a high number of defects and with modified anisotropy necessary for the elimination of hard bubbles. The anisotropy change is the highest at a dose of 2×10^{14} Ne^+ ions/cm^2 (for a strain of 1.1%); at higher doses and strains of about 2.5% (5×10^{14} Ne^+ ions/cm^2) the implanted layer becomes amorphous. Hard-bubble suppression is known to occur for neon implantation doses and energies reported here.[4,14]

Figure 2 shows that a threshold implantation energy of about 30 keV, i.e., a minimum implanted volume, is needed for coercivity reduction, in agreement with hard-bubble suppression experiments. The coercivity remains constant for further increase of the implantation energy up to 120 keV; however, successful hard-bubble suppression was reported for neon energies up to 270 keV.[15]

TABLE II. Average coercivity values for 5-μm SmCaGeYIG epitaxial garnet films (in the upper indices of H_c, s denotes stripe, b bubble, 0 nonimplanted, i implanted samples; n is the number of Bloch lines; d is the bubble diameter.

Film no.	H_c^{s0} (Oe)	H_c^{si} (Oe)	H_c^{b0} (Oe)	H_c^{bi} (Oe)	H_c^{s0}/H_c^{si}	H_c^{b0}/H_c^{bi}	H_c^{b0}/H_c^{s0}	H_c^{bi}/H_c^{si}	n/d (μm^{-1})	n
1	0.25	0.25	0.59	0.44	1.0	1.34	2.36	1.76	7.96	37
2			2.94	2.21		1.33			10.20	62
3	2.08	2.17	2.96	2.39	0.96	1.27	1.41	1.11	8.37	45
4			3.52	2.57		1.37			11.40	54
5			0.62	0.42		1.29			9.48	52

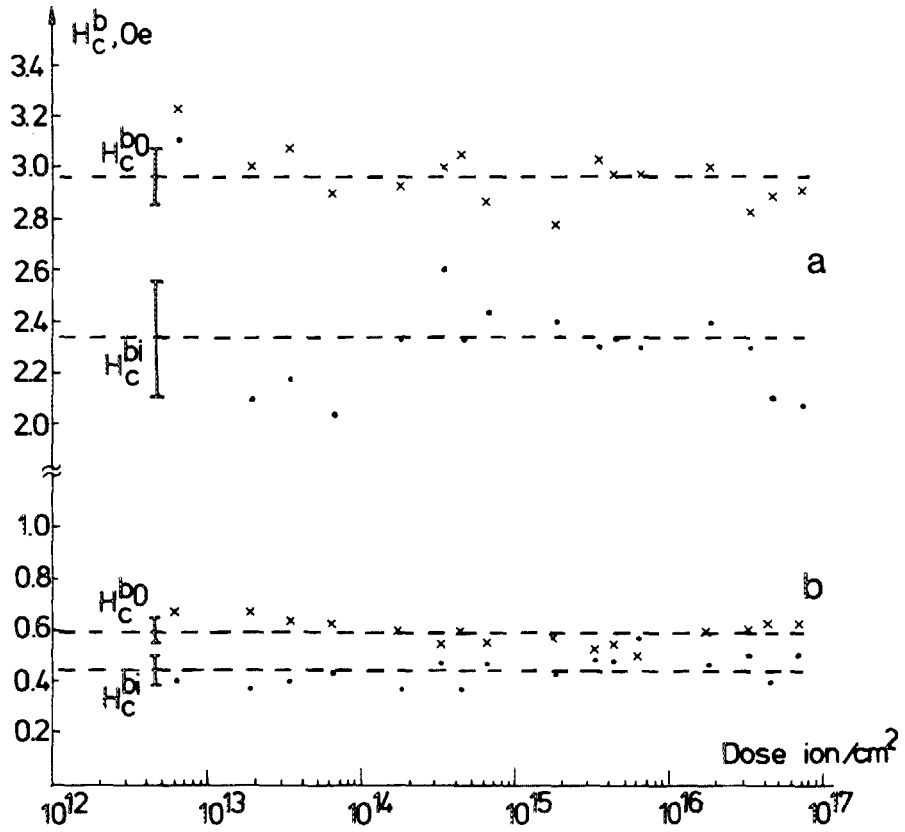

FIG. 1. Dose dependence of static bubble coercivity H_c^b for epitaxial garnets (a) no. 3 and (b) no. 1 for 80-keV Ne^+ ions. ×—H_c^{b0}, ●—H_c^{bi}, measured on the same samples before and after implantation. Broken lines are mean values.

For implantation energies above the threshold value and at low doses, hard bubbles with high collapse field (high ΔH_0) are present; they are absent in the 5×10^{13}–10^{15} Ne^+ ions/cm^2 range; at higher doses ΔH_0 increases again, a phenomenon which was also observed in Ref. 4, and is not fully understood. Comparison of Figs. 1 and 3 shows that the reoccurrence of hard bubbles at higher dose, indicated by increasing ΔH_0, is not followed by a H_c increase. One of the reasons for this may be that visual measurements of ΔH_0 are based on the observation of the highest H_0 for the hardest bubble, while photoelectrical detection of H_c gives average values for a large ensemble of bubbles, and implantation (at

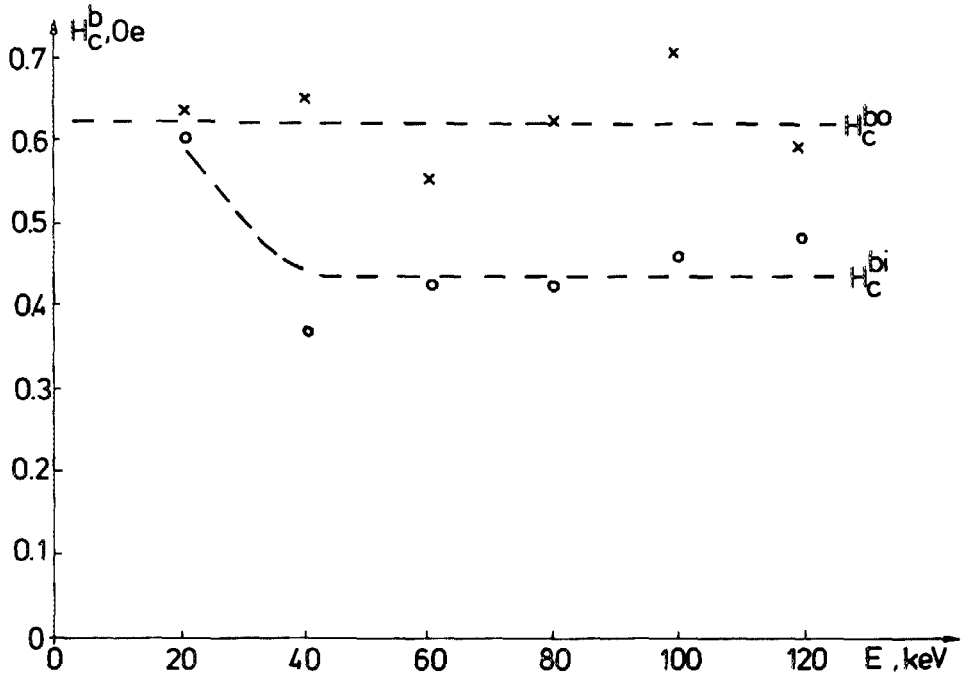

FIG. 2. Implantation energy dependence of bubble coercivity (*no. 5 of Table I*) for implantation with 6×10^{14} Ne^+ ions/cm^2. ×—H_c^{b0}, ○—H_c^{bi}, measured before and after implantation on the same samples.

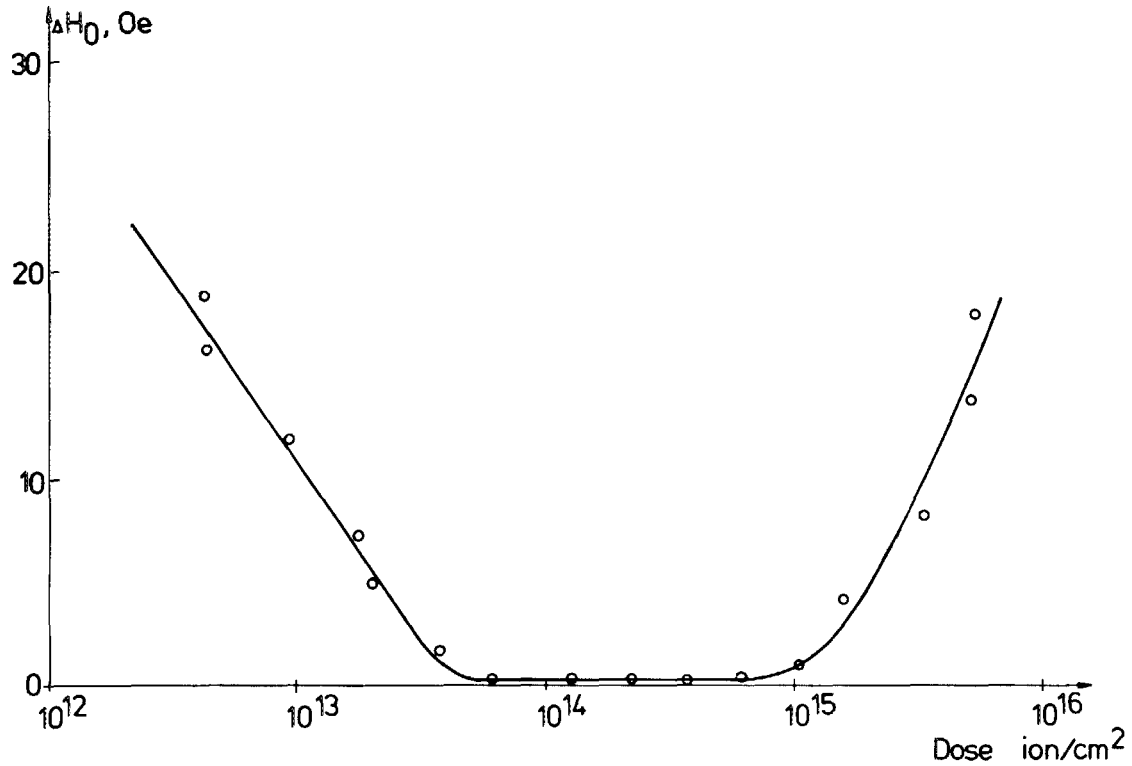

FIG. 3. Collapse-field distribution range ΔH_0 vs implantation dose for 80-keV Ne^+ ions (no. 3 of Table I).

higher doses, too) softens the majority of bubbles. Measuring H_c in nonimplanted samples, the coercivity of bubbles with the average number of Bloch lines is determined.

Coercivity decrease by implantation cannot be explained by classical theories.[16] Inhomogeneous internal strains and possible surface roughening caused by implantation should increase the coercivity. Coercivity can be reduced by decreasing the total domain-wall energy via the reduction of the wall area by the thickness of the implanted layer, supposed to be nonmagnetic. In this case the surface area of a 5-μm-high bubble would be reduced by about 2%, much less than the observed coercivity decrease. Another way for wall-energy reduction is the decrease of its density. The wall-energy density of hard walls, due to the presence of Bloch lines, is always higher than that of normal bubbles. Elimination of hard walls by ion implantation may result in the observed decrease of coercivity.

The contribution of the Bloch lines to the wall energy density of a bubble was calculated by Rosencwaig, Tabor, and Nelson[2] and Thiele,[3] assuming that the total wall energy is the sum of the energies of alternate Bloch and Néel segments. For noncompressed Bloch lines when $d\pi > 2nx_0$ (where d is the bubble diameter, $2n$ is the total number of Néel segments present, i.e. the revolution number, $x_0 = \pi(A/2\pi M_s^2)^{1/2}$ is the length of the individual Bloch line, A is the exchange parameter, and M_s is the saturation magnetization), the wall energy density according to Ref. 3 is given by

$$\sigma_{nc} = \sigma_0\left\{1 + \frac{16A}{\pi Q^{-1/2}\sigma_0}\frac{n}{d}\left[1 + 4\exp\left(-\frac{\pi^2}{2x_0}\frac{d}{n}\right)\right]\right\}, \quad (1)$$

where σ_0 is the wall energy of a normal bubble.

For greater density of Bloch lines, when Néel segments are in contact and Bloch lines are compressed, the wall energy is given by

$$\sigma_c = \sigma_0(\delta_0/\delta_c), \quad (2)$$

where $\delta_0 = \pi(A/K_u)^{1/2}$, or in the terms of the quality factor

$$\delta_0 = \pi\left(\frac{A}{2\pi M_s^2}\frac{1}{Q}\right)^{1/2} = x_0 Q^{-1/2} \quad (3)$$

is the Bloch wall width without Bloch lines. The wall width with Bloch lines is

$$\delta_c^{-2} = \delta_0^{-2} + \left(\frac{\pi}{2}\frac{d}{n}\right)^{-2} \quad (4)$$

and the corresponding wall energy is equal to

$$\sigma_c = \sigma_0\left[1 + \delta_0^2\frac{4}{\pi^2}\left(\frac{n}{d}\right)^2\right]^{1/2} \quad (5a)$$

or

$$\sigma_c = \sigma_0\left[1 + \frac{4x_0^2}{\pi^2 Q}\left(\frac{n}{d}\right)^2\right]^{1/2}. \quad (5b)$$

The ratio of the hard-wall energy to the normal-wall energy as a function of Bloch line number, calculated from Eqs. (1) and (5), is given in Fig. 4 for a typical garnet with $A = 2.2\times10^{-7}$ erg/cm, $4\pi M_s = 200$ G, and $d = 5\times10^{-4}$ cm for various quality factors Q in a range typical for garnet films of this work. For constant material parameters (A, M_s, d, and Q) the hard-wall energy σ_c increases with increasing Bloch line number. For a constant σ_c/σ_0 (at constant A, M_s, and d) the ratio of n^2/Q remains constant, and n increases

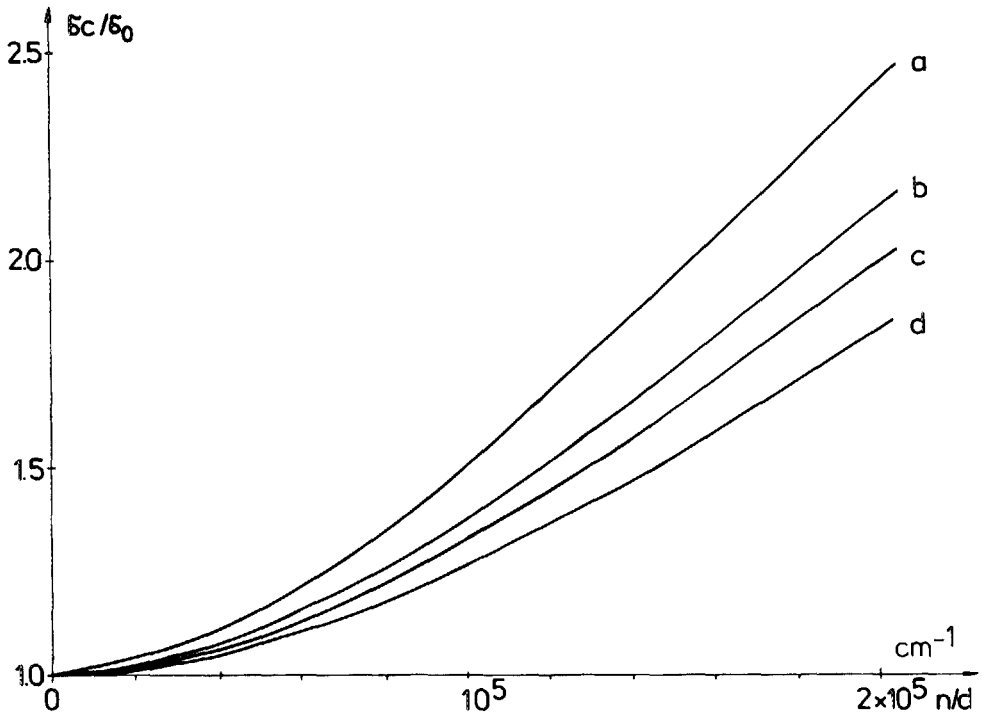

FIG. 4. Relative domain-wall energy density σ_c/σ_0 vs Bloch line density n/d for 5-μm bubbles [Eq. (5)]. $Q = 4.4$, 6.3, 8.2, and 9.4 for curves a–d.

with increasing quality factor, i.e., going from curve a ($Q = 4.4$) to curve d ($Q = 9.4$) in Fig. 4.

For 5-μm bubbles the critical Bloch line density, i.e., the number of Bloch lines when they are continuously wound around the πd perimeter of the wall, is given by

$$\frac{n}{d} = \frac{1}{2}\left(\frac{2\pi M_s^2}{A}\right)^{1/2} \simeq 4.2\times 10^4 \text{ cm}^{-1}.$$

This means that for $n \gtrsim 40$ the compressed Bloch line approximation can be used. Typically, for our samples with wall width $\delta_0 \simeq 1.5\times 10^{-5}$ cm and Bloch wall energy $\sigma_0 \simeq 0.2$ erg/cm^2, the Bloch line length $x_0 \simeq 3.7\times 10^{-5}$ cm, from which it follows that the number of Bloch lines is likely to be greater than 40.

The coercivity is the measure of the change of the wall energy along the path of the wall, $H_c \sim d\sigma/dx$. The position dependence of the wall energy is caused by crystalline defects, surface irregularities, microstructural inhomogeneities, and localized anisotropy changes due to electronic point defects. The defect structure and the potential, where the wall is moving, do not depend on wall structure. For a wall having compressed Bloch lines, Eq. (5) can be written in a modified form as

$$\sigma_c = C_1(n)\sigma_0. \tag{6}$$

The coercivity is $H_c \sim d\sigma_c/dx = C_1(n)d\sigma_0/dx = C_1(n)H_{c0}$, and the ratio of the coercivity of a hard wall to the coercivity of a wall without Bloch lines will be equal to

$$H_c/H_{c0} = C_1(n) = \sigma_c/\sigma_0. \tag{7}$$

For our case H_c/H_{c0} is equal to the bubble coercivity ratio, H_c^{b0}/H_c^{bi}, measured before and after ion implantation.

Table II gives the measured coercivity data together with the ratio of coercivities. From the proportionality given by Eq. (7) the average number n can be calculated using Eq. (5), or Fig. 4 and the parameters given in Table I. The measured samples had nearly identical magnetizations and exchange constants, but widely different coercivities, and their Bloch line numbers n vary from 37 to 62. This number was determined for an ensemble of bubbles on 8–16 samples—with different implantation dosage and energy, but cut from the same epitaxial film—and it has a remarkably low statistical dispersion, the average being for all the measured samples $\bar{n} = (50 \pm 5)\%$. If $n < 15$ then the change of the wall energy (Fig. 4) and the coercivity are within the error limits of our measurements, and a further decrease of the Bloch line number cannot be established by the applied method.

It was assumed that both types of walls contain Bloch lines, viz., the walls of the fully demagnetized stripe domains and the walls of bubbles generated by a pulse modulated bias field by cutting and contracting stripes. However, the number of stripe and bubble Bloch lines may be independent and may fluctuate statistically. Malozemoff[8] determined the contribution to the wall energy caused by the interaction of Bloch lines in stripe domains as an additive term to the normal-stripe coercivity. In this case the stripe-wall energy is given by

$$\sigma^s = \sigma_0^s + \frac{A\pi^2}{hp_0/2}\left(\frac{n}{L}\right)^2, \tag{8}$$

where p_0 is the period of the stripe-domain structure and L the stripe length. As shown by Eq. (8), when the density of Bloch lines n/L is very low, either because of the lower number in stripes than in bubbles, or because of the much greater stripe length compared with the bubble diameter (typically $d/L < 10^{-3}$), the stripe-wall energy will hardly change on implantation—despite the full suppression of hard stripes. In addition, as was shown in the work of Morris, Zimmer, and Humphrey[7] Bloch lines in hard bubbles occur in bundles. In the measurement method of coercivity applied by us, normal-wall segments begin to move before the hard seg-

ments do. The photoelectric detector first senses the motion of the abundant normal walls and thus measures the lowest field for the initiation of normal-wall motion, and the apparent coercivity will be lowered. In the case of the observed number of Bloch lines the bubbles are densely packed by these lines; therefore bubble motion is much more intimately connected with Bloch line motion, and the measured coercivity actually reflects the behavior of these Bloch lines in bubble walls.

It follows from Eqs. (1) and (5) that the wall energy (and in this way the coercivity) depends on the actual bubble diameter and, consequently, on the applied bias field. For a typical 5-μm garnet film with $n = 50$ the change of the bubble diameter by $\pm 1\,\mu$m around the nominal 5-μm value causes σ_c/σ_0 to change by 20%. If the bubble diameter could increase infinitely then $\sigma_c/\sigma_0 \to 1$, and this case would be analogous to a stripe domain. It is widely accepted in the literature that bubble properties like coercivity are treated analytically for symmetrical bubble geometry and, lacking bubble data, the results are compared with stripe measurements. However, the coercivity of bubbles, implanted or not, measured by the same method of quasistatic wall oscillations, is always higher than that of stripes in the same sample. In Walling's paper[17] data are given for both stripe and bubble H_c of unimplanted samples, his H_c^{hyst} being equivalent to our H_c^{s0}, and the higher value of his H_c^{prop}, which is actually the initial field for the motion of an individual bubble, may play the role of our H_c^{b0}. The ratio of his bubble to stripe coercivities varies between 2 and 26, for bubble diameters in the range 1.5–4.1 μm, with a tendency for higher H_c^{b0}/H_c^{s0} for smaller bubbles. Our data for unimplanted materials show a change of H_c^{b0}/H_c^{s0} of 1.5–2.5 for 5-μm bubbles. Unfortunately, to our knowledge no similar data are given in the literature for implanted samples.

While for unimplanted samples a part of the difference between hard-stripe and hard-bubble coercivity is likely to be a consequence of the relative Bloch line density difference of stripe and bubble walls, for the implanted samples this effect is eliminated. The coercivity ratio for our implanted samples, H_c^{bi}/H_c^{si}, varies between 1 and 2. Cape[18] developed a phenomenological model of bubble dynamics in which he treated the various motions of stripes and bubbles. For a wall oscillating in a sinusoidal gradient field the extrapolated intercept in the velocity-versus-drive curve is shown to be $4H_c$ for a bubble and πH_c for a stripe. The ratio $4/\pi = 1.3$ lies in the observed range; however, our results are statistically averaged over many samples with error limits showing that the various ratios of H_c^{bi}/H_c^{si} for various wafers are not due to the scatter of the results. The diameter of bubbles of the measured samples is nearly the same: consequently the change in the radius of curvature or in the wall surface is not the cause of the discrepancy.

V. CONCLUSIONS

The effect of ion implantation on hard-bubble suppresion can be determined by the measurement of the static coercivity, i.e., the field value when quasistatic bubble wall oscillations begin. The effect of implantation with Ne^+ ions on coercivity is independent of the implantation energy and dosage between 40 and 120 keV and in the dose range from 6×10^{12} to 6×10^{16} Ne^+ ions/cm^2, while the collapse-field range ΔH_0 decreases below 2 Oe in a much narrower dose window. The ratio of bubble coercivities before and after implantation is proportional to the ratio of the domain-wall energies with and without Bloch lines. The bubble coercivity after implantation is decreased by about 25% ($H_c^{bi}/H_c^{b0} = 0.76$), remarkably consistent for the measured nominal 5-μm SmCaGeYIG (YIG denotes yttrium iron garnet) bubble materials even though the coercivities H_c^{s0} ranged from 0.6 to 3.5 Oe. From the change of H_c^b on implantation the average number of Bloch lines (n) was determined according to Eq. (5). The n value for the investigated samples varies between 37 and 62, the relative Bloch line density being $8.0 \leqslant n/d \leqslant 11.4\ \mu\text{m}^{-1}$. With constant $H_c^{b0}/H_c^{bi} = \sigma_c/\sigma_0$, the increase of n with increasing Q is seen from the data of Tables I and II.

The coercivity of stripe domains measured before and after implantation did not show any significant change, i.e., $H_c^{s0}/H_c^{si} \simeq 1$. The coercivity change on implantation for hard stripes cannot be revealed by this method because the relatively low Bloch line density in the long stripes causes only a very small increase of the wall-energy density, which is within the error limits of the measurement. In the same way, the presence of a low number of Bloch lines in bubbles—depending on actual material parameters—or the existence of some hard bubbles cannot be determined by static coercivity or collapse-field measurements. The observation that even after the elimination of hard walls the stripe and bubble coercivities are not equal, but $1 < H_c^{bi}/H_c^{si} < 2$, for nearly constant p_0/d for various samples, shows that the usual approximation of applying the results obtained for the case of straight long walls to bubble domains may not always be justified.

ACKNOWLEDGMENT

The authors are grateful to A. A. Thiele for a careful reading of the manuscript and valuable suggestions.

[1] W. J. Tabor, A. H. Bobeck, G. P. Vella-Coleiro, and A. Rosencwaig, Bell Syst. Tech. J. **51**, 1427 (1972).
[2] A. Rosencwaig, W. J. Tabor, and T. J. Nelson, Phys. Rev. Lett. **29**, 946 (1972).
[3] A. A. Thiele, J. Appl. Phys. **45**, 377 (1974).
[4] R. Wolfe and J. C. North, Bell Syst. Tech. J. **51**, 1436 (1972).
[5] H. L. Lu and E. A. Giess, IEEE Trans. Magn. **MAG-11**, 1085 (1975).
[6] S. Konishi, IEEE Trans. Magn. **MAG-19**, 1841 (1983).
[7] T. M. Morris, G. J. Zimmer, and F. B. Humphrey, J. Appl. Phys. **47**, 721 (1976).
[8] A. P. Malozemoff, Appl. Phys. Lett. **21**, 149 (1972).
[9] B. K. Jindal and C. A. Castro, IEEE Trans. Magn. **MAG-16**, 619 (1980).
[10] P. F. Tumelty, R. Singh, and M. A. Gilleo, in *AIP Conference Proceedings No. 29* (AIP, New York, 1976), p. 99.
[11] R. W. Patterson, J. Appl. Phys. **45**, 5018 (1974).
[12] R. M. Josephs, in *AIP Conference Proceedings No. 10* (AIP, New York, 1972), p. 286.
[13] J. A. Seitchik, G. K. Goldberg, and W. D. Doyle, J. Appl. Phys. **42**, 1272 (1971).
[14] P. Gerard, Thin Solid Films **114**, 3 (1984).
[15] G. P. Vella-Coleiro, R. Wolfe, S. L. Blank, R. Caruso, T. J. Nelson, and V. V. S. Rana, J. Appl. Phys. **52**, 2355 (1981).
[16] E. Kneller, *Ferromagnetismus* (Springer, Berlin, 1962).
[17] J. C. Walling, J. Appl. Phys. **50**, 2179 (1979).
[18] J. A. Cape, J. Appl. Phys. **43**, 3551 (1972).